THE JOURNAL OF PHYSICAL CHEMISTRY C
A JOURNAL OF THE AMERICAN CHEMICAL SOCIETY

pubs.acs.org/JPCC

Article

Species Distribution During Solid Electrolyte Interphase Formation on Lithium Using MD/DFT-Parameterized Kinetic Monte Carlo Simulations

Michail Gerasimov, Fernando A. Soto, Janika Wagner, Florian Baakes, Ningxuan Guo, Francisco Ospina-Acevedo, Fridolin Röder, Perla B. Balbuena,* and Ulrike Krewer*

Cite This: J. Phys. Chem. C 2023, 127, 4872−4886

Read Online

ACCESS | Metrics & More | Article Recommendations | Supporting Information

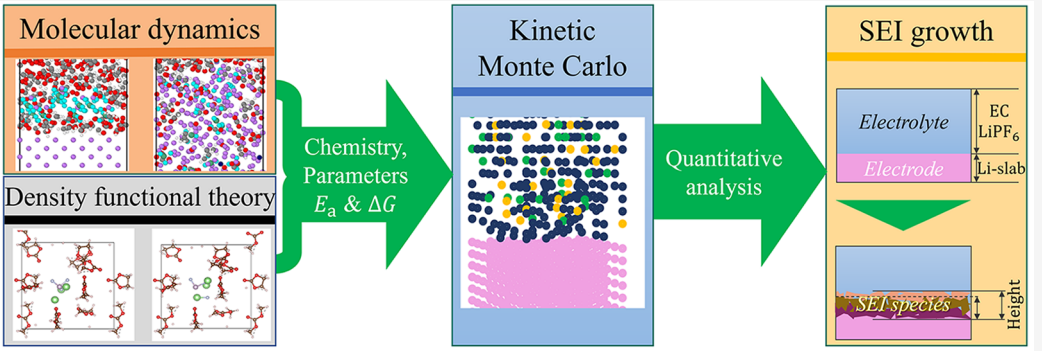

ABSTRACT: Lithium metal batteries are one of the promising technologies for future energy storage. One open challenge is the generation of a stable and well performing Solid Electrolyte Interphase (SEI) between lithium metal and electrolyte. Understanding the complex interaction of reactions at the lithium surface and the resulting SEI is crucial for knowledge-driven improvement of the SEI. This study reveals the internal species distribution and geometrical aspects of the native SEI during formation by model-based analysis. To achieve this, a combination of molecular dynamics, density functional theory, and stand-alone 3D-kinetic Monte Carlo simulations is used. The kinetic Monte Carlo model determines the SEI growth features over a long time and length scale so that the SEI can be analyzed quantitatively. The simulation confirms the frequently postulated layered SEI structure arising from the decomposition of an ethylene carbonate/lithium hexafluorophosphate (2 M) electrolyte with lithium metal. These layers are not clearly separated, which is contrary to what is often reported. The gradient distribution of the species within the SEI therefore corresponds to a partly mosaic structured SEI at the borders of the layers. At the lithium surface, an inorganic layer of lithium fluoride and then lithium carbonate is observed, followed by an organic, more porous SEI layer consisting of lithium ethylene dicarbonate. Simulations further reveal the strong prevalence of corrosion processes of the metal, which provide more than 99% of the lithium for the SEI reaction processes. The salt contributes less than 1% to the SEI formation. Additionally, SEI formation below and above the initial interface was observable. The here presented novel modeling approach allows an unprecedented in-depth analysis of processes during native SEI formation that can be used to improve design for high battery performance and durability.

1. INTRODUCTION

In order to achieve the goals regarding the prevention of climate change, sustainable energy technologies are required. Promising technologies like electric vehicles or electric airplanes especially depend on advancements of electrical storage systems. Thereby, one of the important key indicators is energy density.[1] One promising option is the development of secondary lithium metal batteries for commercial applications. Lithium as a negative electrode material is very interesting since it is an element that has an exceptionally low electrochemical potential (−3.05 V vs standard hydrogen electrode in pure form).[2] In contrast to common lithium-ion batteries, metal batteries do not require a host material like graphite.[3,4] Therefore, lithium metal electrodes are lightweight (0.534 $g \cdot cm^{-3}$) and have a high specific capacity (3.86 $Ah \cdot g^{-1}$). To bring secondary batteries with lithium metal electrodes to the market, scientists continuously investigate methods to solve severe actual problems like dendrite growth[5] or poor cyclability,[6] which presently prevent their commercial usage.

Received: August 17, 2022
Revised: February 2, 2023
Published: March 1, 2023

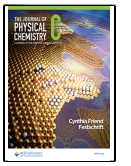

Degradation products from the reduction reactions with or at lithium metal form the so-called Solid Electrolyte Interphase (SEI), a layer covering the anode of the battery.[7] The layer enhances the battery's ability to run safely by protecting the anode's surface from direct contact with the electrolyte, thus preventing uncontrollable reduction of the latter. At the same time, it allows Li-ions to pass.[8] The consumption of Li-ions during its formation causes an irreversible loss of capacity and it acts as an additional internal resistance that decreases battery performance.[9] In general, the SEI can still be seen as the least understood component in the battery, yet one of the most important in terms of extending battery life, leading to a huge research potential in this topic.[10] The challenge to form a stable SEI is further aggravated by the fact that lithium is plated on or stripped from the electrode, causing structural changes during operation.[11] Resulting lithium dendrite formation can lead to a catastrophic failure and degradation up to thermal runaway, e.g., via a short circuit.[4] A stable SEI is the most promising approach to prevent such undesired effects.[1,4]

To tackle those challenges, several experimental and theoretical studies have been performed to analyze the layer, e.g., the structure or formation of the SEI on lithium metal.[2,12,13] In particular, the processes behind the SEI formation are extensively investigated resulting in, e.g., reaction networks explaining the different SEI forming mechanisms.[14] Using continuum models, the autocatalytic effect of HF at higher temperatures could be identified, which convert Li_2CO_3 to LiF.[15] Such investigations of the chemical interactions between species within the battery are useful to provide information about, e.g., the optimal choice of electrolyte and additives[16] for a better performing SEI and battery. Experimentally, electrochemical impedance spectroscopy (EIS) is most commonly used for operando SEI analysis, for instance, for resistance and porosity identification.[17] The combination of discharge curves and EIS has been used to identify with a physical model the thickness, surface roughness, and other properties of the SEI. Those morphological properties can be used for an assessment of the batteries aging process and to develop aging countermeasures.[18] Furthermore, a rougher surface of the SEI increases the probability of losing capacity due to the evolution of dead lithium or increases the batteries safety due to higher likely dendrite growth.[19,20] More in-depth analysis on the surface processes at the SEI and aging are obtainable by Nonlinear Frequency Response Analysis.[21] The method enables separate detection of SEI growth and Li plating and, thus, can be used to mitigate safety-critical plating occurrence.[22] Further insights are obtained by Fourier transform infrared spectroscopy, infrared absorption spectroscopy, Raman spectroscopy, X-ray photoelectron spectroscopy, or X-ray absorption near edge structure.[23]

Today's knowledge indicates that the SEI is a porous mixture of inorganic and organic compounds,[24] whereby the exact composition depends on the electrolyte composition.[13] Furthermore, the internal structure was proposed to be either mosaic-like (randomly mixed) or layered,[25] whereas the exact distribution of species is hardly described.[26,27] Various thicknesses of the SEI, ranging from a few to hundreds of nanometers, are reported,[13,25,26,28] as well as a rough structure and porosity. Despite the large effort, it remains challenging to determine exact values of those parameters.[29] Overall, experimental studies provide much information, however, they are hard to perform in situ and cannot measure the fast reactions and processes during the initial formation process itself, which range from femtoseconds to seconds.

Insights into the processes in the first picoseconds have been gained by simulation approaches such as ab initio molecular dynamics (AIMD) on the atomistic scale. They focused on the initial reduction of the electrolyte describing the electrolyte decomposition on lithium, carbon, and silicon electrodes.[30−32] The studies revealed the electrolyte decomposition as a function of lithiation, electrolyte solution and salt concentration and other characteristics, in a very small time scale of picoseconds.[32,33] Moreover, classical reactive molecular dynamic simulations have been successful in capturing the evolution of the interfacial region including lithium oxidation, penetration of electrolyte molecules, and the initial formation of SEI products.[34] More recently, Ospina-Acevedo and coworkers used a combined MD/DFT approach to characterize the nucleation of SEI components such as lithium fluoride (LiF).[24] Despite the tremendous success in characterizing the SEI via AIMD simulations, the approach is also limited in the number of molecules in the system as well as simulated time. The simulated times for AIMD simulations only reach hundreds of picoseconds at best. Thus, the aggregation of SEI species to clusters, comparable to crystal growth, is not observable at time scales covered by AIMD, e.g., the formation of lithium fluoride (LiF) clusters. Classical MD[24] can reach the order of nanoseconds but requires careful force field parametrization. Moreover, quantitative morphological analysis like the SEI thickness or structure is difficult when using MD simulations. However, physicochemical parameters are extractable for usage in models of longer time scales. A further group of SEI models is taking a macroscopic view and use continuum and mean-field models which do not resolve stochastic molecular processes but use mean-field approaches.[18,35] Clusters or other heterogeneities in the SEI are not covered by such models and thus cannot give an in-depth perspective.[36]

A modeling methodology bridging the scale of molecular and continuum, i.e., macroscopic modeling, is essential to understand formation of the heterogeneous SEI structure including clusters. Mesoscale models like kinetic Monte Carlo (KMC) allow to close this gap. SEI formation and coverage of the (carbon) electrode was modeled, including electrochemical reactions.[37−39]

The method was further extended to model the formation of an SEI on graphite in a full Li-ion battery including a complex multistep mechanism.[36,40] Extension to the full cell level was thereby achieved with a multiscale 2D+1D model, which coupled the KMC model for SEI growth with a continuum model for the battery. In our previous work,[36] we could show with this model not only the evolution of thickness, reaction rates and composition of the SEI for a full battery charge, but also that a decrease in graphite particle size leads to significantly more capacity loss due to more SEI growth. The model was extended to locally 2D+1D discretized electrodes, which allowed to see the effect of charging rate on homogeneity of SEI growth along the thickness;[41] whereas low currents lead to high uncertainty in compositions, high currents lead to higher SEI thicknesses close to the separator.

Furthermore, hybrid models like the Red Moon methodology (a combination of MD and KMC simulation) were also used successfully to describe SEI formation. It is able to switch from MD simulations directly to a KMC simulation in one box such that a higher validity than stand-alone KMC models can

https://doi.org/10.1021/acs.jpcc.2c05898
J. Phys. Chem. C 2023, 127, 4872−4886

be reached.[42] Using this methodology, Takenaka et al. were able to describe the first steps of SEI formation with a higher number of atoms and larger time scale such that chemical processes of different electrolytes can be analyzed and compared to each other. For instance, the solvent EC seems to form a more stable SEI than PC. However, this requires again much higher computational costs such that the time scale is smaller than the stand-alone KMC methodology.[43]

To summarize, the successful application of KMC for studying the SEI formation in graphite electrodes of Li-ion batteries clearly demonstrates the potential of KMC for studying surface changes at long time scales (up to hours) and length scales (up to micrometers), which cannot be reached by DFT, AIMD, or similar methods. Yet, our previous 2D+1D KMC models assumed a flat graphite electrode of unchanged structure. Modeling of lithium metal, however, would need to take into account surface changes of lithium due to reactivity. Further, whereas SEI builds up slowly on graphite electrodes and only when decreasing potential below 0.05 V vs Li/Li^+,[44] SEI formation on lithium is a rapid process that instantaneously starts upon contact with electrolyte.[14]

Here, we present the first stand-alone 3D KMC model to study the SEI formation on lithium metal in contact with organic electrolyte, to reach unprecedented time and length scales, and quantitative information for the species distribution and morphology. For establishing and demonstrating the method, we choose a simple, well studied electrolyte, $LiPF_6$ in ethylene carbonate (EC) and omit any additives.

Most of the required parameters defining the rates of single reaction processes were taken from literature or determined by DFT and AIMD simulations. Using these for KMC simulations allows us to present insights into the SEI's internal structure and 3D spatial distribution. Moreover, we are extending the analysis to larger length and time scales than pure AIMD/MD simulations. For the first time, therefore, we will give an insight into the SEI composition regarding structure, especially its temporal evolution of the species distribution. Moreover, structural properties like SEI porosity or thickness are analyzed which are crucial for further battery development.

2. METHODS

2.1. General Reaction Model. First, the general model setup for both, MD/DFT and KMC is described. MD/DFT simulations are generally more precise than KMC models regarding molecular interactions. However, they cannot provide quantitative information on the products' long-term evolution and their spatial distribution due to box size and time limitations. In contrast, KMC may overcome these restrictions but requires the input of basic thermodynamic and kinetic parameters to simulate the SEI growth. Consequentially, by using the output of the thermodynamic and kinetic parameters of MD/DFT simulations directly as an input for the KMC model, both models' strengths can be combined. A graphical illustration of the scenario and model approach for the SEI growth is shown in the graphical abstract.

As the MD/DFT and KMC need to be based on the same reaction network, the chosen reactions for the simulation have to be selected first. The modeled scenario is as follows: a pure lithium metal is dipped into an electrolyte consisting of ethylene carbonate and 2 M lithium hexafluorophosphate ($LiPF_6$) as salt. Therefore, a native SEI can be formed due to the thermodynamic instability of the electrolyte. No electric field is applied, and all reactions are spontaneous. The respective chemical equations are summarized in Table 1 and are graphically depicted also in the SI, Scheme S1. The choice of those reactions is based on the widely accepted degradation reactions for ethylene carbonate and $LiPF_6$ reported by previous investigations as well as our own MD simulations.[8,14] Those reactions can be divided up into two main SEI-forming paths: The EC-reductive path, reactions R1−R7, and the salt-reactions path, reactions R8−R13, see Table 1.

Table 1. Chemical Reactions Considered for the SEI Growth[a]

No.	reaction
R1	$C_3H_4O_3 + e^- \rightleftharpoons C_3H_4O_3^-$
R2	$C_3H_4O_3^- + Li^+ \rightleftharpoons LiC_3H_4O_3$
R3	$2LiC_3H_4O_3 \rightleftharpoons (CH_2OCO_2Li)_2 + C_2H_4$
R4	$C_3H_4O_3^- + e^- \rightleftharpoons CO_3^{2-} + C_2H_4$
R5	$Li^+ + CO_3^{2-} \rightleftharpoons LiCO_3^-$
R6	$LiCO_3^- + Li^+ \rightleftharpoons Li_2CO_3$
R7	$LiC_3H_4O_3 + e^- \rightleftharpoons LiCO_3^- + C_2H_4$
R8	$Li^+ + PF_6^- + e^- \rightleftharpoons LiF + PF_5^-$
R9	$Li^+ + PF_5^- + e^- \rightleftharpoons LiF + PF_4^-$
R10	$Li^+ + PF_4^- + e^- \rightleftharpoons LiF + PF_3^-$
R11	$Li^+ + PF_3^- + e^- \rightleftharpoons LiF + PF_2^-$
R12	$Li^+ + PF_2^- + e^- \rightleftharpoons LiF + PF^-$
R13	$Li^+ + PF^- + e^- \rightleftharpoons LiF + P^-$
R14	$LiF + Li^+ + e^- \rightleftharpoons Li_2F$
R15	$Li_2F + Li^+ + e^- \rightleftharpoons Li_3F$
R16	$Li_3F + Li^+ + e^- \rightleftharpoons Li_4F$

[a]A graphical illustration is provided in the SI, Scheme S1.

EC reduction is commonly accepted as being responsible for a part of the SEI formation.[10] In general, it starts with the EC reduction via an electron, which is considered in reaction R1. The initial reduction is followed by one of two possibilities: The first is a reaction of $C_3H_4O_3^-$ with lithium (reaction R2), forming $LiC_3H_4O_3$, which in literature is assumed to be the pre stage of the reaction to $(CH_2OCO_2Li)_2$ (reaction R3).[45] The second one is another follow-up reduction of the one-time reduced EC to form CO_3^{2-} (reaction R4). In this case, reaction R5 with one lithium ion leads to $LiCO_3^-$, which can further react via reaction R6 to the second main SEI species, Li_2CO_3, as reported in former studies.[46] Some investigations report the possibility of $LiC_3H_4O_3$ to react to $LiCO_3^-$ via a reduction, which is considered in reaction R7.[14,45,47]

The salt reactions start off with the well-known salt dissociation, which is taken into account via reaction R8.[48] However, Martinez de la Hoz et al. reported a further breakdown of the PF_5^- molecule by releasing fluorine atoms, which was the reason to consider this process via reactions R9−R13.[33] Since recent AIMD simulations showed a further reaction of LiF, we allowed further association of the LiF molecule with other lithium atoms up to Li_4F, denoted in reactions R14−R16.[24] Note that Li_xF refers to a coordination number x of the lithium with one fluorine atom. Even though a coordination number up to six was reported,[24] no parameters

https://doi.org/10.1021/acs.jpcc.2c05898
J. Phys. Chem. C 2023, 127, 4872−4886

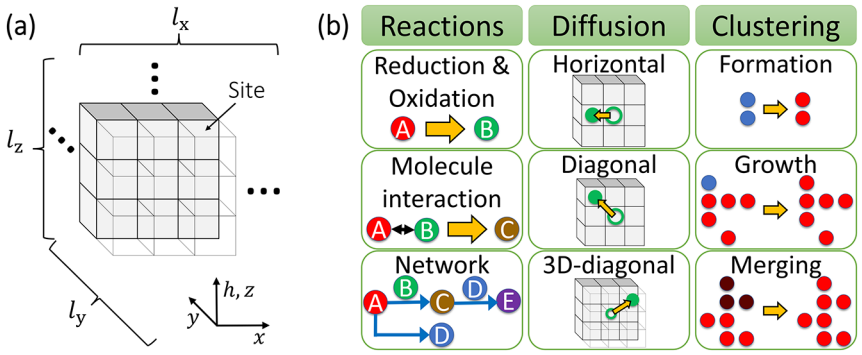

Figure 1. (a) Basic KMC box illustration. (b) Modeled processes in the KMC simulation. Reactions: The letters indicate different types of molecules. Diffusion: Movement of a molecule from one site to another. Clustering: Clusters are marked in (dark) red, nonclustered molecules are shown in blue.

could be obtained for such high coordination numbers, which led to the decision to exclude five and six.

The origin of the lithium for the reactions is still under discussion: It can possibly come from the anode or the electrolyte, whereas the corrosion of Li metal is mostly assumed as prevalent.[14] Besides the here considered reaction sequence, other reactions and intermediates have been postulated or reported but will be not considered in this study.[45] This is because the respective species required for the reactions are either present in smaller traces in the SEI only, or because they stem from impurities (such as water), or are part of cathode degradation. Impurities and crosstalk from the cathode are known to impact the SEI[8,49] but impurities are neglected in this first study and no cathode is present in our scenario. Also, species not considered include the SEI molecules Li_2O, which is often reported to be formed in batteries,[46] as it requires free oxygen atoms to be present in the system, which are expected at higher salt concentrations.[50]

Finally, the following general assumptions regarding the reactions have been considered:

- The lithium metal consists of pure lithium without any external impurities due to, e.g., oxidation. The electrolyte is assumed to have no impurities like water.
- Lithium is always able to be oxidized spontaneously to $Li^+ + e^-$. This is assumed since a metal in contact with an electrolyte always oxidizes to a certain degree depending on its electrochemical stability.[51] This effect was also shown via MD simulations indicating that the oxidation barrier for lithium is very low.[24] Thus, lithium metal atoms can spontaneously react with species analogously as Li^+.
- All reactions occur at 25 °C, since the AIMD parameters were obtained at the same temperature.
- Gaseous species are not modeled, as they are assumed to be inert and be removed instantaneously from the surface into the cell. Similarly, a pressure increase due to gas evolution is neglected.
- The following species are considered as SEI species: $(CH_2OCO_2Li)_2$, Li_2CO_3, Li_3F, and Li_4F. Their clusters are assumed to be in a solid state and are able to be part of the SEI layer on lithium metal.

2.2. MD/DFT Model. For the MD/DFT part of the model, the focus lies on the determination of the parameters required as inputs for the KMC simulation, especially the activation energy E_a and free energy $\Delta_r G$. Energies for the solvent, reactions R1, R3, and 4R, could be obtained by previous investigations, the values for reactions R2 and R5−R7 were chosen in the range of the ones provided by literature due to computational restrictions. For the determination of the free energy $\Delta_r G$ of the lithium salt decomposition reactions R8−R13, the slow-growth approach was used, which is a constrained AIMD methodology and further described in section 1.2, SI. For reactions R14−R16, increasing the number of lithium atoms that are assigned to one fluorine atom (reactions), the activation energies and free energies were chosen in the range of the reported ones in ref 24. The concrete values for all reactions can be found in the SI, Table S1.

Finally, for the assessment of the percentage of every SEI species within the KMC-simulated SEI, a volume calculation for the real molecular sizes were obtained. The methodology is described in section 1.3, SI, as well as the results in SI, Table S2.

2.3. KMC Model. Using the molecular modeling methods of section 2.2, all energy parameters for the reactions in Table 1 were determined and are given in Table S1, SI. In the next step, the obtained activation and free energies from the DFT simulations are transferred to the KMC model for simulating the SEI growth. In the following, the KMC box setup will be described, cf. Figure 1a.

Similar to MD simulations, the KMC simulation uses a 3D-box and it contains a fixed number of cubic cells within a lattice with length x, width y, and height z. On each lattice site, a maximum of one molecule may be placed that is a state-of-the art procedure in KMC simulations.[52] Thus, every molecule of the system requires exactly one site to be placed within the cell. The distance between two lateral cells, and thus the size of a single cell, Δl, is set constant to 0.3443 nm. This is within the range of the reported values of an optimized lithium bulk crystal.[53] Further, this distance is the smallest one in the whole box.[54] Therefore, this distance assures the most compact box which is possible. Moreover, since geometries of molecules are not considered, a finer grid supports in-directly the fact that a nonplanar molecule has always a smaller cross-sectional surface area than a planar molecule. This leads to the conclusion that nonplanar molecules are closer to each other supporting the choice of a small site distance. Box dimensions are $l_x = 15\Delta l = 5.1645$ nm, $l_y = 15\Delta l = 5.1645$ nm, and $l_z = 75\Delta l = 25.8225$ nm, as the larger dimension of l_z permits growth of the SEI especially in the direction of z, perpendicular to the initial interface of electrode/electrolyte at height z_{II}. For easier understanding and assessment of the results, the height can

https://doi.org/10.1021/acs.jpcc.2c05898
J. Phys. Chem. C 2023, 127, 4872−4886

also be expressed with the layer number $h = z \cdot \Delta l^{-1} \in \mathbb{N}$. The dimensions were chosen since they provide enough space for possible inhomogeneities and quantitative evaluation of the SEI and do not limit its formation (cf. section 3.1), but are not larger than required such that computational costs can be saved. For the initial configuration of the KMC box, all cells below z_{ll} = 10.329 nm constitute the pure lithium electrode. Consequentially, the initial height of the pure lithium corresponds to $h_{ll} = z_{ll} \cdot \Delta l^{-1}$ = 30 layers. The large number ensures sufficient space for the SEI to grow not only on top of the initial electrolyte phase ($z > z_{ll}$) but also, via corrosion, below the initial surface into the metal ($z < z_{ll}$).

The electrolyte and conductive salt are placed above the last initial lithium layer until the top of the box at $z = l_z$. Not every cell in the electrolyte phase is occupied with electrolyte or salt. The amount of electrolyte molecules N_{EC} and amount of salt molecules N_{salt} which need to be placed can be calculated via eq 1:

$$N_i = \lfloor N_a \cdot c_i \cdot l_x \cdot l_y \cdot (l_z - z_{ll}) \rfloor \tag{1}$$

where $i \in \{EC, Li^+, PF_6^-\}$, N_a is the Avogadro constant, and c_i expresses the concentration of either the solvent or a salt ion. The salt concentration was set to 2 M. We assume a complete salt dissociation of the $LiPF_6$ to Li^+ and PF_6^-. Pure EC equals to a concentration of 15 M. However, as some sites of the electrolyte phase are taken by the salt and thus reducing the concentration of EC within the electrolyte, the concentration of EC is reduced by the mols of salt and thus is set to 11 M. Thus, 55.8% of the sites above the lithium metal remain empty in the initial box. Note that the voids are an artifact of the static 3D KMC grid, as all molecules occupy the same volume of one site within the KMC box. Finally, the boundary conditions need to be defined. For the four outer surfaces perpendicular to the metal−electrolyte interface, i.e., x−z at $y = 0$ and $y = l_y$, and y−z at $x = 0$ and $x = l_x$, respectively, periodic boundary conditions are used. Movement across the planes are not interfered, and the molecule would appear then at the lateral plane. This decision was taken since it can be assumed that next to the modeled box other boxes of the same type are present. At $z = 0$, hard-wall conditions are used to account for Li metal continuing below $z = 0$ in real systems. Yet, molecules at $z = 0$ can move to a different x and/or y coordinate. At the top of the box ($z = l_z$), an open boundary condition is set where a bulk electrolyte is assumed with a constant concentration of solvent and salt ions (corresponding to 2 M $LiPF_6$). This triggers diffusion processes over the boundary, when species are consumed or produced in the box. Molecules may leave the box through the top of the KMC box, and fresh electrolyte (EC, Li^+, PF_6^-) may enter without restrictions via diffusion, as would also occur in real systems. This allows particles to possibly exchange between the box and the bulk phase.

As discussed in section 2.1, evolving gaseous species are not considered. The system itself is operating under open circuit conditions, thus no potential dependency of reactions is considered, and no forced (dis)charging reactions, e.g., Li^+ reduction to Li. Effects of electric fields are also not considered at this stage as well so that electroneutrality within the box is not enforced. Implementing electroneutrality will require significant additional effort in method development by extending KMC or coupling to a continuum model, as done in our prior multiscale battery works.[36,40]

The KMC algorithm (flow diagram see SI, Scheme S2) is based on a Markov chain approach and uses a variable step size method,[55] which works for every time step as follows: First, transition rates $W_{j,i}$ for every possible process j of every molecule i are determined. If a process requires more than one site or molecule, the algorithm checks whether the condition of a site/molecule being present is satisfied. If not, the transition rate is set to zero. The transition rate is also set to zero for a void site. A probability $\mathcal{P}$ for a process to happen can be calculated via dividing the sum of transition rates of the process j for all molecules by the sum of all transition rates of all processes Ω:

$$\mathcal{P}_j = \frac{\sum_i (W_{j,i})}{\Omega} = \frac{\sum_i (W_{j,i})}{\sum_j \left(\sum_i (W_{j,i})\right)} \tag{2}$$

Then, a process is chosen that is going to be executed. This choice takes place randomly, but considers the probabilities of the processes and the respective number of molecules. In a third step, a molecule in the process is chosen that executes the process. To select the molecule, which executes the chosen process, a second random number is drawn and used to determine the respective molecule out of those being capable of performing the process. If the process requires additional specifications again this is made randomly. This is used, for instance, for diffusion to determine in which possible directions the chosen molecule shall diffuse or for reactions, if several species next to the chosen molecule are available. After executing the process at the chosen place, the elapsed time during this step is calculated. The corresponding time step size is calculated by dividing the negative logarithm of a randomly chosen number ξ between 0 and 1 by the sum of all transition rates at the time step:

$$\Delta t = -\frac{\log(\xi)}{\Omega} \tag{3}$$

Other methodologies using sampling are also mentioned in the literature, whereby some of them incorporate additional features of the species. However, in order to reduce computational time as much as possible such that the high time and length scales can be achieved, a rejection-free methodology needed to be taken. Furthermore, sampling methods like transition path sampling require additional knowledge about the products within their transition states during reaction. Since such features depend heavily on the environmental conditions (charges, geometry of molecules etc.) and thus increase the complexity heavily, this method is not suitable for being applied on stand-alone KMC systems like the SEI formation presented here.

The KMC model contains three main microscopic process categories: reactions, diffusion, and clustering (cf. Figure 1(b)). Reactions follow the reaction network that was previously introduced in Table 1. Diffusion describes the movement of molecules from one site to a neighboring site, whereby horizontal movements in either x, y or z direction, diagonal movements in xy, xz or yz direction, or 3D-dimensional movements in xyz are considered. The travel distance for every type corresponds to the distances in the box calculated via Pythagoras's theorem: $\Delta l_{horizontal} = \Delta l$, $\Delta l_{diagonal} = \sqrt{2} \cdot \Delta l$ and $\Delta l_{3D\text{-}diagonal} = \sqrt{3} \cdot \Delta l$.

Lastly, clustering of the solid SEI species $(CH_2OCO_2Li)_2$, Li_2CO_3, Li_3F, and Li_4F is considered. Clustering describes the accumulation of solid species by structural reorientation of the

https://doi.org/10.1021/acs.jpcc.2c05898
J. Phys. Chem. C 2023, 127, 4872−4886

affected molecules.[56] Clusters can either be formed, extended, or merged together with another one, as displayed in Figure 1b.

In the following, details on the three process categories are given.

2.3.1. Reaction. Intermolecular reactions are a major part of the SEI growth since they allow the formation of various new solid SEI species.[46] The transition rate W of any of the considered reactions can be calculated via the respective reaction rate constant k:

$$W_r = k \tag{4}$$

All reactions can occur in the forward and backward direction apart from those that require gaseous species. If a reaction is not equimolar, neighboring void sites are produced or occupied by a new molecule, respectively. To determine the reaction rate constant for a forward reaction, k_f, and backward reaction, k_b, transition state theory is used:[57]

$$k_f = \sigma(h)\cdot k_0 \cdot e^{-E_a/(R\cdot T)} \tag{5}$$

$$k_b = \sigma(h)\cdot k_0 \cdot e^{-E_a/(R\cdot T)} \cdot e^{\Delta_r G/(R\cdot T)} \tag{6}$$

The activation energies E_a and free energies $\Delta_r G$, which were derived from the DFT calculations, literature or literature-based chosen (section 2.2 and SI, section 1.2), are used as input in eqs 5 and 6. Their values are noted in the SI, Table S1. The frequency factor k_0 is set constant to 10^{13} s^{-1}, following the harmonic transition state theory.[58] Finally, for reactions involving electrons, the electron tunneling from the surface of the lithium metal to a molecule in the electrolyte at height h of the KMC box is modeled by the electron factor σ. It constitutes the probability of the existence of free electrons at a given position in the lattice relative to the surface. As several reactions depend on the presence of electrons (cf. Table 1), their corresponding rates are sensitive to the electron factor. In order to model it for the whole KMC box, the electron factor is defined to depend on the distance from the location to the initial surface layer of the lithium metal anode grid, h, and is modeled as follows (derivation see SI, section 1.5):

$$\sigma(h) = \begin{cases} 1, & h < h_{ll} + 1.5 \\ (h_{max} - h_{ll} - 1.5)\left(\frac{\ln(p_{max})}{e^{h_{max}-h_{ll}-1.5}} - 1\right)e^{\frac{\ln(p_{max})(h-h_{ll}-2)}{h_{max}-h_{ll}-1.5}} \\ \hline \ln(p_{max}) \end{cases}, \quad h \geq h_{ll} + 1.5 \tag{7}$$

Thereby, the constant parameters h_{ll} and p_{max} describe the position of the initial lithium anode layer at the interface to the electrolyte-filled layer and the probability for an electron tunneling up to the layer $h_{max} = 34$, respectively. Note that the electron factor σ is only applicable for reactions containing an electron within the reaction equation. For chemical reactions, where no external electrons are needed, the electron factor is set to one.

2.3.2. Diffusion. Diffusion is implemented as a stochastic, spontaneous process, following the concept of Brownian motion. It can only occur in the liquid phase, i.e., between sites that do not contain solid species. As this will lead to even distribution, no further concentration gradient needs to be considered. The transition rate for diffusion of a molecule to a new site depends on the distance between the two sites and number of unoccupied neighboring sites. The diffusion coefficient of all species, D, was set to a constant value of $1.8 \cdot 10^{-10}$ m^2 s^{-1}, which is in the range of reported values for EC systems.[59] Barriers hindering the diffusion in the electrolyte at surfaces, such as the Ehrich-Schwoebel barrier occurring at step sites[60] were not considered. It is assumed that the increase of required energy for diffusion at surfaces, which equals to a lower transition rate, is sufficiently accounted for by the longer diffusion distance. This leads to the transition rate of diffusion as defined by[61]

$$W_{d,horizontal} = N_{void}\cdot\frac{D}{(\Delta l_{horizontal})^2} \tag{8}$$

$$W_{d,diagonal} = N_{void}\cdot\frac{D}{(\Delta l_{diagonal})^2} \tag{9}$$

$$W_{d,3D\text{-}diagonal} = N_{void}\cdot\frac{D}{(\Delta l_{3D-diagonal})^2} \tag{10}$$

with Δl as the distance of the two sites' centers and N_{void} the number of void neighbors.

2.3.3. Clustering. Finally, clustering describes the process of forming solid amorphous or crystalline structures of SEI species from all possible neighboring solid species of the same kind which was already observed via MD simulations[50] and experimentally for, e.g., LiF.[62] It is assumed that clustering corresponds to an irreversible intramolecular diffusion process, similar to an internal molecule rearrangement observed in ref 56. Since a rearrangement optimizes the energy state of the species to a final configuration, clusters were included in this study. Only the solid SEI species $(CH_2OCO_2Li)_2$, Li_2CO_3, Li_3F, and Li_4F can form clusters. Clusters are defined to consist of the same kind of species only. Since the process is most similar to a diffusion process,[56] the transition rate for the clustering of two species was defined by the same equation as for the diffusion itself:

$$W_{cl,horizontal} = N_{i,horizontal}\cdot\frac{D}{(\Delta l_{horizontal})^2} \tag{11}$$

$$W_{cl,diagonal} = N_{i,diagonal}\cdot\frac{D}{(\Delta l_{diagonal})^2} \tag{12}$$

$$W_{cl,3D\text{-}diagonal} = N_{i,3D\text{-}diagonal}\cdot\frac{D}{(\Delta l_{3D\text{-}diagonal})^2} \tag{13}$$

with N_i referring to the number of clustered neighbors. Note that a clustered species cannot diffuse any more, as this would interfere with its assumed optimized position and energy state.

2.3.4. Implementation and Parameter Set. The chosen parameter set for the simulation is given in Table 2.

Due to the sequential processing of the KMC algorithm, computational power is crucial for a fast and detailed calculation. In our model, the KMC simulation and all related calculations were implemented in MATLAB R2020b code[64] and executed on an Intel i7-6700K six core processor. The simulation was stopped after 7.500.000 iterations corresponding to ca. 100 ns. This resulted in a computation time of roughly 2 days for 7.500.000 iterations of the variable step size algorithm, which is a long computational time compared to continuum simulations,[65] but not to AIMD simulations. To provide values for statistic uncertainty analysis, the KMC

https://doi.org/10.1021/acs.jpcc.2c05898
J. Phys. Chem. C 2023, 127, 4872−4886

Table 2. Set of Parameters of the KMC Simulation

parameter	variable	value	source
diffusion constant in EC	D	$1.8 \cdot 10^{-10}$ m^2 s^{-1}	chosen in the range of[59]
diameter of molecule	d	0.5 nm	chosen
activation energy	E_a	see SI, Table S1	see SI, Table S1
free energy	$\Delta_r G$	see SI, Table S1	see SI, Table S1
initial last lithium metal layer	h_{ll}	30 (≙10.329 nm)	chosen
last significant tunneling layer	h_{max}	34 (≙11.706 nm)	chosen
reaction rate constant	k	calculated	eqs 5 and 6
frequency factor	k_0	10^{13} s^{-1}	chosen (cf.[63])
lateral distance of two sites	Δl	0.3443 nm	chosen in the range of[53]
length of the simulation box	l_x	5.1645 nm	chosen
width of the simulation box	l_y	5.1645 nm	chosen
height of the simulation box	l_z	25.8225 nm	chosen
probability of electron at last significant tunneling layer	p_{max}	0.01	chosen
temperature	T	298.15 K	chosen
transition rate	W	calculated	eqs 4, 8, and 11
electron factor	σ	calculated	eq 7

simulations were repeated with the same initial setup eight times.

2.3.5. Evaluation and Interpretation. In the following, we explain how the simulated data is postprocessed to determine chemical composition of the resulting SEI as well as the geometric properties of the SEI morphology.

By definition, molecules are considered as being part of the SEI if they fulfill two conditions: First, they have to belong to one of the clustered SEI compounds $(CH_2OCO_2Li)_2$, Li_2CO_3, Li_3F, and Li_4F. Second, they are either one layer away from the electrode or connected to it via other clustered SEI molecules. The fraction of a compound i in the SEI in layer h, $p_{h,i}$, is determined from the number of molecules of compound i in this layer $N_{h,i}$ divided by the total number of clustered SEI molecules in this layer $N_{h,SEI}$:

$$p_{h,i} = \frac{N_{h,i}}{N_{h,SEI}} \tag{14}$$

The following morphology analysis evaluates (local) height and porosity of the SEI. This can only be a rough estimate, as we apply some simplifications due to the KMC-typical assumption of an equidistant grid: each place contains either one molecule or is void, and all particles, except for clusters, or sites are assumed to occupy the same molecule size. Taking into account the differences of real particle sizes would lead to a distorted grid, with immensely increased complexity and computation time.

For the morphological analysis, the maximum SEI height R_{max} can be obtained by eq 15.

$$R_{max} = z_{max,SEI} - z_{min,SEI} + \Delta l \tag{15}$$

It describes the height difference from the layer where the first SEI molecule appears $z_{min,SEI}$ to the uppermost layer in the direction z, where an SEI molecule is found, which is still $z_{max,SEI}$ in the z-direction, connected to other neighboring SEI species.

Moreover, the mean height of the SEI, $\bar{R}$ is calculated by using the following equation:

$$\bar{R} = \frac{1}{N_h} \cdot \sum_{(x,y)} (z_{max,SEI,(x,y)} - z_{min,SEI,(x,y)} + \Delta l) \tag{16}$$

In this formula again, the difference between the lowest molecule and highest molecule is taken, but here for all sites with the coordinates (x,y). This sum is afterward divided by the total number of sites per layer N_h.

To calculate the volume fraction of the SEI, the outer boundaries of the SEI need to be defined. The volume fraction evaluation starts at the first layer, where SEI species occupy at least 5% of the voxels within a layer. This amount of SEI is defined to be significant. The last considered layer is the one which also satisfies the condition and is connected via layers below to the first one, which also contain at least 5% of SEI species. All clustered species are counted and divided by the total number of sites. This method of calculation ensures that only the SEI-containing layers are considered. This method might lead to some noise within the graph for layers close to the 5% boundary.

As the last parameter, the area specific capacity loss $C_{A,loss}$ due to the consumed lithium metal is calculated. Using the number of consumed lithium metal atoms $N_{Li,consumed}$, $C_{A,loss}$ can be obtained by the following equation:

$$C_{A,loss} = \frac{N_{Li,consumed} \cdot \Delta l^3}{l_x \cdot l_y} \cdot \varrho_{Li} \cdot C_{m,Li} \tag{17}$$

Here, ϱ_{Li} equals the density of pure lithium (0.534 g·cm^{-3}) and $C_{m,Li}$ is the mass specific capacity of lithium (3.86 Ah·g^{-1}).

3. RESULTS AND DISCUSSION

In the following, we first will analyze the evolution of the SEI on the pristine lithium surface to get an insight into the interaction of processes and the forming of characteristic phases in the SEI. Subsequently, we analyze the resulting SEI layer to get information about structure and morphology.

3.1. SEI Growth and Species Distribution. In the following, the growth of the SEI on a native lithium metal surface exposed to electrolyte containing EC and 2 M $LiPF_6$ is discussed. Focus is on formation of the initial SEI layer. Snapshots of the distribution of the most relevant species for the initial configuration and that after 102.8 ns are given in Figure 2. Illustrations of the KMC boxes with all species can be found in the SI, Figure S1. During the last 10% of the simulation time, no further SEI change occurred. This can be attributed to the stop of reactions creating new SEI which is caused by blocking of further electrolyte coming sufficiently close to lithium for reacting (further explanation will be provided later in this chapter). Thus, the initial SEI formation can be seen as completed and the simulation was stopped. It is very probable that further SEI growth and possibly changes in structure and composition will take place after the initial formation, but over a much longer time period in the range of seconds and more. The processes occurring at the longer time scale are not in the focus of our study, as they are of a different nature, including further reaction of solid species, as well as further electron transport processes.[66]

In the initial state, lithium metal has a thickness of 10.329 nm and is in its upper layer in contact with the electrolyte, which is composed of EC and the dissociated salt,

https://doi.org/10.1021/acs.jpcc.2c05898
J. Phys. Chem. C 2023, 127, 4872−4886

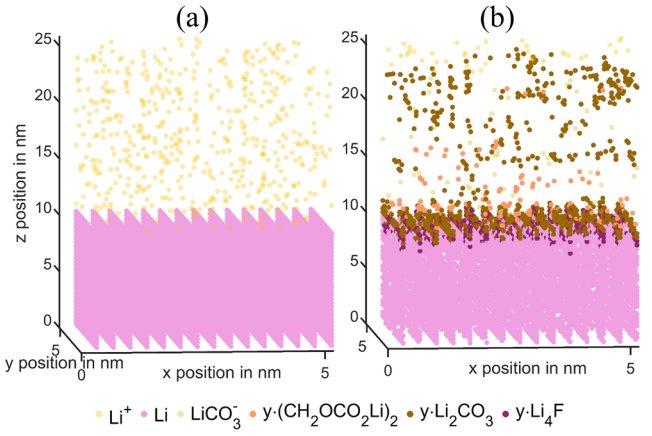

Figure 2. Change of species distribution at the lithium-electrode interface due to reactions that lead to the build-up of the solid electrolyte interphase at T = 298.15 K, open circuit potential, using pure EC and c_{LiPF_6} = 2 M. (a) Initial configuration; (b) Configuration at 102.8 ns.

$LiPF_6$. Only the upmost layer is in contact with the electrolyte, and species within the electrolyte are homogeneously distributed. The simulation after 102.8 ns shows at the interface a ca. 3 nm thick layer composed of clustered Li_2CO_3 and Li_4F and an on-top layer of $(CH_2OCO_2Li)_2$. Further, it can be seen that no significant amount of clustered Li_3F is present.

The SEI layer is formed above and below the original interface at t = 0 due to the following reason: lithium metal is oxidized by the electrolyte species, leading to a corrosion effect. The newly observable corrosion of the electrode results in a formation of the SEI products below the initial surface position. Further, electrolyte species are reacting at the surface, leading to decomposition products above the original interface position. Besides a strong accumulation of reaction products at the interface, reaction products can be seen to be distributed widely over the electrolyte. This can be explained by diffusion: nonclustered SEI products $(CH_2OCO_2Li)_2$, Li_2CO_3, and Li_4F are produced in the electrolyte at the interface to solid SEI or lithium. They need to cluster with a molecule of the same species in order to be part of the SEI and fixed in their position (cf. section 2.1). This probability depends highly on the number of clusters of the same species being neighbors. There is also a probability that they rather diffuse within the electrolyte. In the electrolyte they may form clusters at higher layers once they meet other species, often after much longer time. A similar effect was observed in our prior studies for SEI formation on carbon,[36] where significant portions of SEI products did not precipitate at the surface, but accumulated in the electrolyte. The SEI formed at the lithium surface has a layered structure with a gradient in composition. It starts with clusters of Li_4F at the lithium metal surface, followed by Li_2CO_3 clusters and finally $(CH_2OCO_2Li)_2$ clusters. The model thus suggests a formation of an inorganic inner SEI layer, consisting of Li_4F and Li_2CO_3 and an outer organic one consisting of $(CH_2OCO_2Li)_2$, which in general fits to suggested SEI models in literature.[25,26] The simulated distribution confirms the experimental reports of a rather layered SEI structure of inorganic SEI at the electrode surface followed by an organic layer. However, the distinction of the layers is not clear and the species distribution at the edges is rather blurred. As the results here refer to very small time scales, this implies that the SEI species composition reported in the literature[14] is not an effect of SEI aging over longer time only. Rather, the SEI immediately contains all species, and the direct pathway from EC to Li_2CO_3 seems to be significant.

Additionally, lithium from the metal is displaced toward the electrolyte phase during the simulation. It is visible in the final configuration as shown in Figure 2b: the SEI species are located above the initial interface between the electrode and electrolyte. This results from diffusion of lithium atoms into the electrolyte so that the respective SEI species can be formed above the initial interface. The mechanism was similarly reported in the literature.[24,34] The salt's lithium can also be part of formed SEI species. However, less than 1% of the lithium in the final SEI can be attributed to this source in our simulation. This is the first simulation-based confirmation of the open question and claim by He et al.[14] that while most SEI forming reactions are facultative corrosive, i.e., they might use Li metal or Li from electrolyte, initial SEI formation on lithium metal is predominantly a corrosion process. The main reason for that is the high local availability of lithium metal at the initial metal/electrolyte interface, where most of the SEI is formed. After 102.8 ns, the SEI clusters consist of ca. 56% Li_2CO_3, followed by approximately 25% Li_4F and ca. 19% $(CH_2OCO_2Li)_2$ related to the amount of total SEI molecules. Unclustered SEI species are present but are less than 1% of the entire SEI. This implies, that the species tend to cluster rather than to stay unclustered.

A small number of Li_2CO_3 molecules are present above the SEI layer at all height coordinates of the box, and especially close to the top boundary. This can be attributed to the effect of the top boundary condition: lithium ions of the salt react with CO_3^{2-} at the top of the box, leading to Li_2CO_3 via reactions R5 and R6.

To understand the evolution of the SEI structure, to identify the main reactions that lead to the observed SEI, and to determine their contribution throughout the simulated growth period, we analyze the SEI evolution over time more deeply. In Figure 3, results for two additional times, 0.4 and 41.4 ns, are shown. Here, the time 0.4 ns corresponds to the start phase of SEI formation, and thus, a comparison with the SEI at 102.8 ns allows the identification of the first reactions. 41.4 ns corresponds to ca. 40% of total elapsed time and, thus, allows to see if the build-up of the SEI is still in strong progress or if composition and growth have already settled.

In Figure 3a,b, the distribution of the selected species within the KMC box is depicted. The figure shows solid SEI products and additionally $LiCO_3^-$. The visualization containing all species can be found in the SI, Figure S3. Figure 3c,d further gives a quantitative insight into the distribution of clustered SEI formation products vs height. Here, the number of molecules of a given species in each layer was multiplied by the true volume of the respective molecule (see SI, Table S2) to determine the expected volume fractions of species over height. This was motivated by the fact that $(CH_2OCO_2Li)_2$ molecules are 94% larger than Li_2CO_3, and 147% larger than Li_4F. The dashed lines illustrate the observed SEI borders, which were the outermost layers with at least 5% of SEI species and the initial lithium metal/electrolyte interface.

In Figure 3a, it can be seen that already after a very short time a significant amount of SEI and other reactant species have been formed at the Li−metal/electrolyte interface. Shortly after the first reduction of EC to EC^-, it reacts with

https://doi.org/10.1021/acs.jpcc.2c05898
J. Phys. Chem. C 2023, 127, 4872−4886

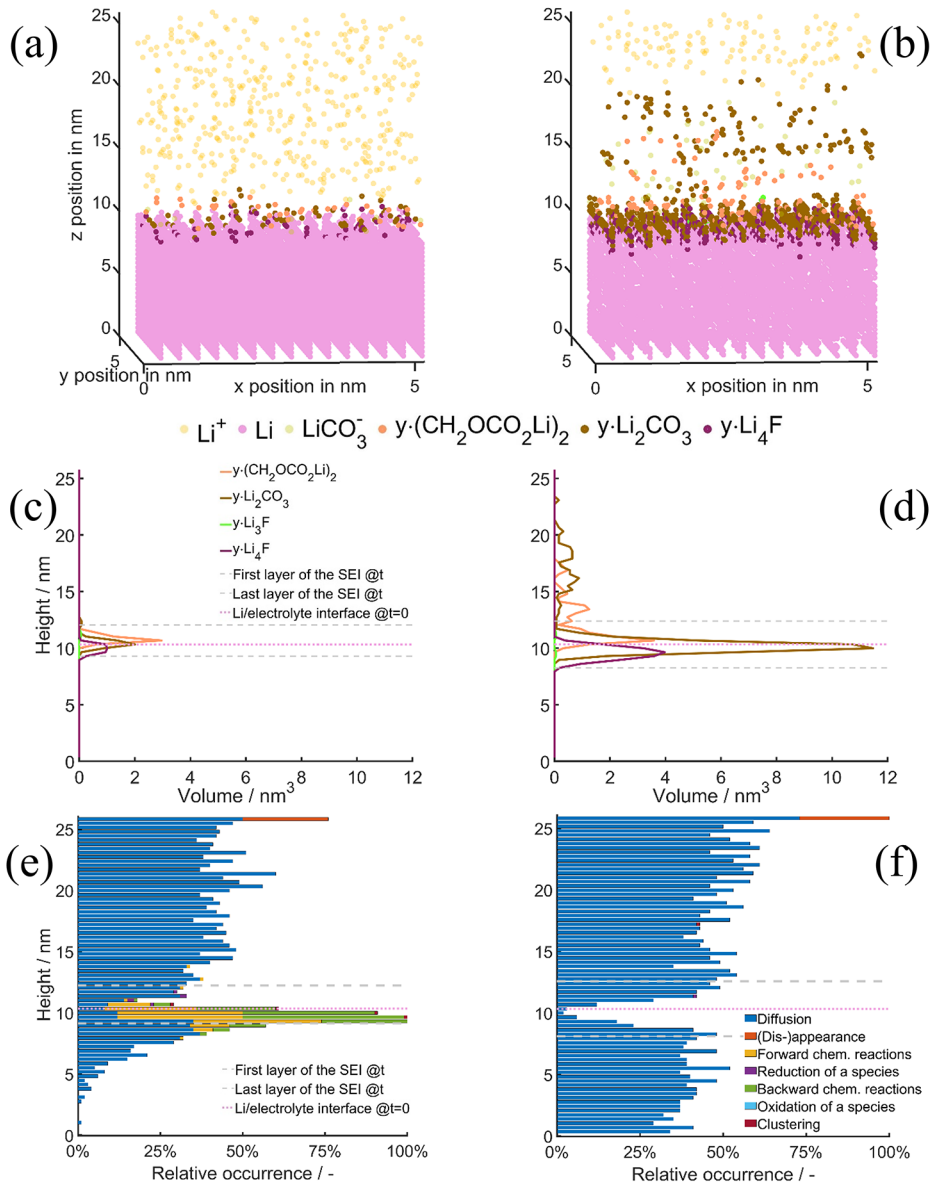

Figure 3. Progress of the SEI formation process at T = 298.15 K and c_{LiPF_6} = 2 M after 0.4 ns (left) and 41.4 ns (right). (a, b) KMC with distribution of selected molecules; (c, d) Volume occupied by the solid SEI species at a given height. The area between the two gray lines constitutes the solid SEI layer where clustered species are connected; (e, f) Relative occurrence of processes over height. 100% corresponds to the layer with the highest amount of the total processes occurring.

lithium metal to yield $LiC_3H_4O_3$ within the electron tunneling range, highlighting the importance of the electron factor mentioned in section 2.3.1. Subsequently, $LiC_3H_4O_3$ reacts rapidly to $(CH_2OCO_2Li)_2$ (Figure 3a). In parallel, Li_2CO_3 is formed after a second reduction of EC. The additional reduction step of EC^- to CO_3^{2-} possesses a further reaction barrier. Thus, it makes formation of Li_2CO_3 less likely than of $(CH_2OCO_2Li)_2$, which is indicated by the higher reaction rate of $(CH_2OCO_2Li)_2$ shown in SI, Figure S5. Note that there are two reaction pathways for the reduction of EC^-, which might form $LiCO_3^-$: either via CO_3^{2-} (reactions R4 and R5) or via $LiC_3H_4O_3$ (reaction R7). Simulation results reveal that the reduction reaction of $LiC_3H_4O_3$ (reaction R7) to $LiCO_3^-$ occurs extremely seldomly (less than one reaction (reaction R7) every 10 ns), indicating that this reaction is less relevant for the initial SEI formation. The probability of the second reduction of EC^- by reaction R4 is less likely than the formation of $(CH_2OCO_2Li)_2$ via reaction R3. In comparison to Li_2CO_3 and $(CH_2OCO_2Li)_2$, lithium fluoride requires a slightly longer time until it is produced due to a high activation energy. Thus, there is only little Li_4F present after 0.4 ns. Because the formation of Li_4F requires twice the amount of lithium atoms than the other SEI species, it is mostly formed at the lithium metal interface where more lithium atoms are available such that the transition rates of forming Li_4F are much higher.[24] To investigate the occurring processes at each layer, Figure 3e shows the relative occurrence of the processes per layer. It can be seen that all aforementioned reactive processes occur close to the interface, where they lead to the formation of the initial SEI. Thus, prevalence of the reactions directly at the electrode and not in the electrolyte can be confirmed. The reason for the dominance of the reactions over

https://doi.org/10.1021/acs.jpcc.2c05898
J. Phys. Chem. C 2023, 127, 4872−4886

the diffusion and clustering close to the electrode is caused by transition rates for reactions, W_r, being higher than for diffusion, W_d, and clustering, W_{cl}. This is illustrated exemplarily for $N_{void} = 1$.

$$W_r = k = k_f = \sigma(h)\cdot k_0 \cdot e^{-E_a/(R\cdot T)} = 1\cdot 10^{13}\ s^{-1}\cdot e^{-10\ kJ\cdot mol^{-1}/(8.314\ J\cdot mol^{-1}\cdot K^{-1}\cdot 298.15\ K)} \approx 1.77\cdot 10^{11}\ s^{-1}$$

$$W_{d,horizontal} = W_{cl,horizontal} = N_{void}\cdot \frac{D}{(\Delta l_{horizontal})^2} = 1\cdot \frac{1.8\cdot 10^{-10}\ m^2\cdot s^{-1}}{(0.3443\ nm)^2} \approx 1.52\cdot 10^9\ s^{-1}$$

As $W_r > W_{d,horizontal} = W_{cl,horizontal}$, it can be stated that if a reaction is possible, it is preferred over diffusion and clustering. Further away from the interface, mostly diffusion occurs as very few intermediate species are present. Reactions occur mostly close to the metal/electrolyte interface within the tunneling range of ca. 1.4 nm. At the lowermost and uppermost SEI layer facing Li-metal and electrolyte, respectively, reaction and diffusion occur, both with diffusion supplying new reactants. As a consequence, reactions are the most dominant process, whereas diffusion is the growth limiting one during the first 0.4 ns. Due to the short electron tunneling range, the species being formed are quite close to each other. Thus, clustering already occurs at this early stage. The higher the number of molecules of the same kind, the higher the probability for them to cluster. Therefore, $(CH_2OCO_2Li)_2$ can cluster easily compared to Li_2CO_3 and Li_4F.

Whereas $(CH_2OCO_2Li)_2$ was the most rapidly formed SEI component until 0.4 ns, the situation changes afterward. The formation rate of $(CH_2OCO_2Li)_2$ decreases, while the inorganic amount of the SEI is increasing, cf. SI, Figure S5. This effect can be explained as follows: After Li_4F and Li_2CO_3 formed on the surface of the electrode, they hamper the possibility of lithium metal to take part in the reactions. The SEI hampers transport and reduces the possibility that the one-time reduced EC^- meets a lithium ion. Consequentially, the organic $(CH_2OCO_2Li)_2$ cluster growth via reactions R2 and R3 slows down, whereas the growth of Li_2CO_3 and Li_4F continues, since they are slightly closer to the electrode (Figure 3c). The formation of new Li_4F at the lower end of the SEI can also be related to the literature-mentioned bottom-up SEI growth mechanism, where a growth of the SEI from the lithium metal anode is proposed.[67] A further effect contributes to the preference of $LiCO_3^-$ over $(CH_2OCO_2Li)_2$ formation after 0.4 ns: the closer the EC^- molecule is to the initial surface, the more probable becomes the second EC reduction via reaction R4, resulting in CO_3^{2-} due to the higher value of the likelihood of electron tunneling (see eq 7).

To conclude, the high availability of electrons and decreasing mobility of lithium due to the formed SEI are the reasons why the formation of Li_2CO_3 above the initial metal surface is generally more favorable than the one of $(CH_2OCO_2Li)_2$, at 41.4 ns. Finally, as Li_xF is located directly on the metal surface, it can still grow to $Li_{x+1}F$ since its reactiveness vs $(CH_2OCO_2Li)_2$ is even less limited by lithium diffusion. Nevertheless, Li_xF has higher energy barriers and there is an increasing hampering of the PF_x^- diffusion. Thus, the cluster formation of Li_4F decreases with increasing amount of formed Li_2CO_3. Note that the effect of building SEI on top of present layers or filling up pores within the SEI is not in line with the previously mentioned bottom-up mechanism.[14,66] Therefore, we suggest that both mechanisms are occurring during the native SEI formation, whereas the bottom-up mechanism is driven by Li_4F formation and the building-up mechanism by the formation of Li_2CO_3. We note that Li_4F is only an intermediate species that can be seen for the formation of LiF nuclei.

The change of circumstances just described is reflected in Figure 3b,d,f, showing the simulation results after 41.4 ns. As it can be seen in Figure 3b, Li_2CO_3 is the main SEI species at this time, followed by lithium fluoride. Also, the order of SEI species over its height is now similar to the one of the final results (cf. Figure 2b). Since the blockage of lithium diffusion by Li_2CO_3 at 41.4 ns is very high, the reaction rates of the $(CH_2OCO_2Li)_2$ and Li_2CO_3 formation at the metal/electrolyte interface decrease significantly (cf. Figure 3f). Thus, diffusion is the most frequent process at this time frame, and SEI growth at 41.4 ns and afterward is limited by reactions. In addition, the diffusion causes the following effects. First, a rearrangement process in the lithium metal occurs (section 3.2), which did not exist in the first time frame. Second, the doubly reduced CO_3^{2-} diffuses into the electrolyte and reacts with the salt's lithium above the SEI to Li_2CO_3. Consequentially, Figure 3b,d and very notably the final SEI in Figure 2b show the resulting spread of Li_2CO_3 in the electrolyte layer ca. 5−10 nm above the initial interface after 41.4 ns.

Summarizing, the initial SEI forms instantaneously after very few nanoseconds of contact of electrolyte and lithium, and it follows a specific species sequence of Li_4F, Li_2CO_3, and $(CH_2OCO_2Li)_2$ starting from the metal toward the electrolyte. This order is consistent with findings using hybrid MD/KMC methodologies.[43] The main source of the lithium for the SEI is corroded lithium metal. SEI growth is limited by diffusion at first, which however changes after roughly 41.4 ns to a reaction limited SEI growth. The blocking of the SEI leads at the end of the simulation to no further formation of SEI, since the lithium metal and electrolyte are completely separated by the SEI without any path for the molecules to come close to each other and react (cf. SI, section 2.5). Future research may focus on a longer time scale during SEI formation and aging, as well as what happens with the SEI during operation.

3.2. SEI Structure Analysis. KMC simulations also provide information regarding the morphology of the SEI, such as thickness and porosity, which we will analyze in the following. Yet, we assume a lattice grid with equal space occupied by each molecule, whereas real molecules have different sizes. The macroscopic properties resulting from KMC should thus be seen as indicators of quantitative values.

The first evaluated property is the height of the SEI. Figure 4 displays the evolution of the height of the SEI with time; it shows the maximal height of the SEI, R_{max}, as well as the mean height of the SEI, $\bar{R}$, calculated by equations 15 and 16, respectively. Please note that we only count those solid molecules as part of the SEI that are clustered and connected to a solid neighboring molecule at the neighbor site. Solid products from SEI formation on top of this height, as, e.g., is visible in Figure 2b for Li_2CO_3 at a distance of 5−15 nm above the initial lithium layer, are discounted, as they are only loosely bound to the solid SEI layer.

The maximum SEI height R_{max} increases asymptotically and monotonously to a value of 3.4 nm at 5 ns, which is in the lower range of reported SEI thicknesses[10] but roughly in the same range as observed in other theoretical studies.[43] Moreover, new insight regarding the mechanisms leading to this SEI growth can be shown. Especially the geometrical and

https://doi.org/10.1021/acs.jpcc.2c05898
J. Phys. Chem. C 2023, 127, 4872−4886

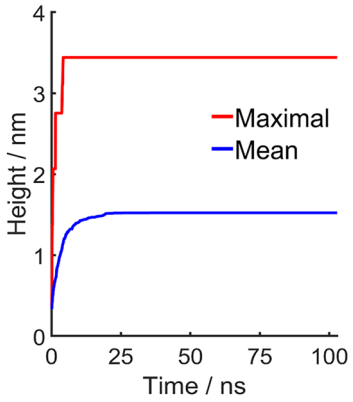

Figure 4. Evolution of maximal and average height of SEI over time during the SEI formation process for T = 25 °C, 2 M $LiPF_6$ in EC.

compositional structure still changes after 5 ns: The mean height of the SEI $\bar{R}$ indicates a slowing growth of the SEI to a steady state value of roughly 1.5 nm at 25 ns. Reason for the longer growth of $\bar{R}$ vs R_{max} is Li_2CO_3 clustering. Li_2CO_3 clusters are the largest and fastest cluster-growing species at 25 ns (more detail in the SI, section 2.3). The total height does not increase due to the limitations of the diffusion explained in section 3.1.

Note that in the simulation electron tunneling was considered as the only electron transport process, whereby the probability for a transport at 1.5 nm equals <3%. This can be calculated via the electron factor σ. Thus, the identified heights of 1.5 nm for the mean and ca. 3.4 nm for the maximal height of the SEI corresponds well to the mostly accepted electron transfer pathway.[66] Other electron transport mechanisms have been postulated, e.g., diffusion or migration,[66] but such processes are thought to depend on charge transfer processes with, for instance, Li-ions or charged fragments. Since those mechanisms are much slower,[66] they do not influence the native SEI formation in the simulated time frame of 102.8 ns. They are thus not considered for our studies on the initial SEI formation. Yet, they may explain the experimentally observed further SEI growth at much larger time scales of minutes and days.

The second analyzed parameter is the volume fraction of the SEI. In Figure 5a, the evolution of the overall SEI volume fraction is shown. According to Figure 5a, the mean SEI volume fraction increases asymptotically within the first 25 ns up to 39.5% and it remains constant subsequently. Note that the high volatility of the volume fraction within the first 10 ns is caused by new clustered species that get connected to the main SEI, and thus suddenly count as SEI henceforth.

Figure 5b depicts the heterogeneous volume fraction distribution of every SEI species as well as the lithium over height. It can be seen that the SEI volume fraction at each layer increases over time due to the higher amount of solid SEI species. Moreover, the spatial distribution of the SEI volume fraction of the single species highly varies, whereby the distribution of SEI species corresponds to the layered SEI structure described in section 3.1. As the mean value stays constant after roughly 25 ns, Figure 5b implies that SEI volume fraction changes only locally after 25 ns.

The low porosity at the initial metal/electrode interface also confirms the previous discussion that reactions slow down due to limited diffusion close to the layer at z = 10 nm. The LiF and Li_2CO_3 layers are so dense that only roughly 10% of the

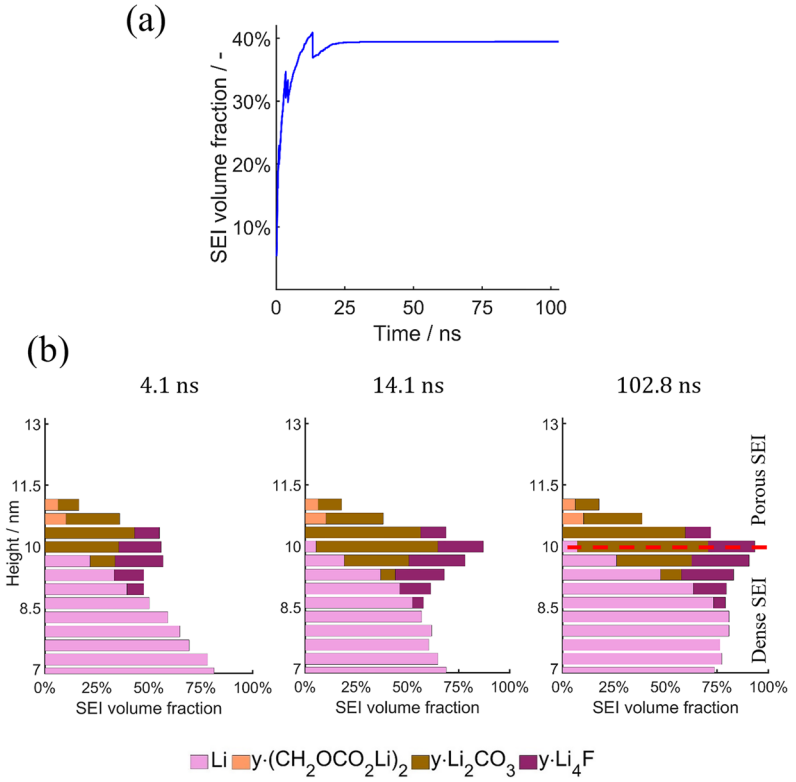

Figure 5. SEI volume fraction over time. (a) Overall mean SEI volume fraction. (b) Volume fraction by SEI species and lithium over height: (1) After 4.1 ns; (2) After 14.1 ns; (3) After 102.8 ns. The red dashed line separates the regions of dense and porous SEI.

https://doi.org/10.1021/acs.jpcc.2c05898
J. Phys. Chem. C 2023, 127, 4872−4886

layer is not occupied by those species at 102.8 ns. Note that the remaining 10% are mostly closed pores not connected to the external electrolyte. Electrolyte molecules which are completely enclosed by nonreactive clustered SEI molecules are unable to diffuse or participate in any reaction. This is further elaborated in section 2.5 and especially Figure S6 of the SI. Overall, the results are in good accordance with literature reports that suggest a denser inner layer close to the anode and a more porous outer SEI.[68,69]

As lithium is consumed during the SEI formation, the volume fraction of lithium decreases heavily in the beginning of the simulation. Due to the high reaction rate during the first nanoseconds, much lithium of the lithium metal/electrolyte interface gets quickly consumed such that further lithium metal atoms move from the lithium bulk toward the top of the anode. This leads to the low volume fraction of lithium at 4.1 ns in Figure 5b. These sites are partially filled with electrolyte molecules which diffused to the sites. Note that due to the solid lithium diffusion, the volume fraction of lithium metal increases afterward over time, leading to the higher volume fraction of lithium at 102.8 ns than at 4.1 ns. Nevertheless, this process also leads to vacancies within our simulation which refer to (temporal) defects within the lithium metal.

Evaluating the difference between the number of initial lithium metal sites and after 102.8 ns, one can assess the capacity loss within that time. Using eq 17, the capacity loss caused by the consumption of lithium due to SEI growth can be determined to approximately 6.69 $\frac{\mathrm{mAh}}{\mathrm{m}^2}$. Applied to a typical battery electrode thickness of 30 μm[70] pure optimized lithium electrode, this would correspond to a lithium inventory and capacity loss due to SEI formation of roughly 0.01%.

4. CONCLUSIONS

Using a combination of MD/DFT and 3D-KMC SEI simulation, our work succeeded in shedding light onto the initial SEI formation on lithium metal in contact with electrolyte. The new methodology not only includes reaction and diffusive processes but also particle clustering leading to an authentic native SEI formation.

Based on our results, we suggest a build-up of a layered structure of the SEI via bottom-up and building-up mechanisms within the first 100 ns, when bringing lithium in contact with EC/$LiPF_6$ electrolyte. The layered SEI species structure is interdiffusing the layers and has different compositions, with the majority of species in each layer being respectively Li_4F, Li_2CO_3, and $(CH_2OCO_2Li)_2$, starting from the lithium metal toward the electrolyte. The relative amount of precipitated or formed solid species in the total SEI after 102.8 ns are 25% for Li_4F, 56% for Li_2CO_3 and 19% for $(CH_2OCO_2Li)_2$. The characteristic distribution of these species originates from the interaction of reactions and diffusion during the formation process: It starts off with the reduction of EC. At this stage, lithium is present next to the reduced EC, leading to a high reaction rate of forming $(CH_2OCO_2Li)_2$, located slightly above the initial interface. The formation of Li_2CO_3 requires the energetically less favorable second EC reduction. This reaction process is most dominant as soon as the Li-ion concentration has been significantly reduced. For Li_4F, the high number of reaction steps with high energy barriers leads to a low reaction rate in the beginning. After this initial phase, the continuous formation of solid Li_2CO_3 and Li_4F hampers the diffusion of EC^- and lithium, resulting in a decreasing production rate of $(CH_2OCO_2Li)_2$. As a result, the SEI gets more inorganic over time. Due to the high lithium consumption when forming Li_4F, Li_4F is located below the initial interface. As a high electron availability is favorable for Li_2CO_3 formation, Li_2CO_3 is in between $(CH_2OCO_2Li)_2$ and Li_4F. Analyzing the source of the lithium for the SEI formation, we reveal that 99% of it can be attributed to lithium metal corrosion and only a small fraction to decomposition of salt from the electrolyte. SEI formation on lithium is thus essentially a corrosion process due to the electrolyte.

Results from the simulated SEI species distribution may be used in future to determine the conductivity and thus the resistance of the SEI. However, the vice versa calculation of SEI composition from a high frequency resistance value from impedance spectra is not feasible.[18] The consumption of the anode leads to a capacity loss of roughly 6.69 $\frac{\mathrm{mAh}}{\mathrm{m}^2}$. Furthermore, the evaluation of the simulated SEI morphology confirmed that it is a porous layer with porosities of 15−35%. This can be further subdivided into a dense inner and a more porous outer layer. Thus, our result supports the by now widely assumed concept of a layered dense-then-porous SEI model. The SEI height converges to a mean height of 1.5 nm and a maximum height of 3.4 nm. The maximum SEI height is limited first mainly due to the short electron tunneling distance. Afterward, only the mean height increases via internal diffusion and clustering until the diffusion of the species from and to the anode is limited and stops the SEI growth completely. The further growth may stem from SEI species within the electrolyte that diffuse through the electrolyte, until they meet a solid SEI component where they cluster.

The presented work reveals the initial SEI formation during the first ca. 100 ns and allows an unprecedented quantitative insight. In this study we used ab initio parameters from different sources with different assumptions. Accuracy of the simulation results may be improved when using a consistent set of ab initio parameters and diffusion coefficients that reflect the local environment. This is significantly more work, but as kinetic parameters may strongly depend on the environment, it may be rewarding, and we expect possible changes in SEI properties and prevailing reactions. Additionally, concepts for maintaining local electroneutrality of the system or ionic conductivity of the SEI need to be considered for longer time scales beyond ns.

The here-presented framework and modeling approach may be extended to analyze further phenomena: for a simulation of a Li-SEI interphase under operation, the present model would need to be enhanced toward lithium plating/stripping and SEI rearrangement. A further extension may comprise simulating a longer exposure of lithium and the SEI to electrolyte, and thus long-term growth. Here, further electron transport paths and reactions may be considered, too.

With our work we would also like to inspire the scientific community to conduct further KMC simulations of electrochemical systems with other salts and solvents. These again would trigger further tailored MD/DFT simulations.

■ ASSOCIATED CONTENT

Supporting Information

The Supporting Information is available free of charge at https://pubs.acs.org/doi/10.1021/acs.jpcc.2c05898.

https://doi.org/10.1021/acs.jpcc.2c05898
J. Phys. Chem. C 2023, 127, 4872−4886

Reaction network, including corresponding energies and clustering processes; Molecular volume calculation; Variable step size methodology for the KMC simulation; Derivation of the electron factor; KMC boxes at different time frames and cross-sectional views; Analysis of the clustering processes and reaction rates (PDF)

AUTHOR INFORMATION

Corresponding Authors

Ulrike Krewer − *Institute for Applied Materials − Electrochemical Technologies, Karlsruhe Institute of Technology, Karlsruhe 76131, Germany;* orcid.org/0000-0002-5984-5935; Email: ulrike.krewer@kit.edu

Perla B. Balbuena − *Department of Chemical Engineering, Texas A&M University, College Station, Texas 77843, United States;* orcid.org/0000-0002-2358-3910; Email: balbuena@tamu.edu

Authors

Michail Gerasimov − *Institute for Applied Materials − Electrochemical Technologies, Karlsruhe Institute of Technology, Karlsruhe 76131, Germany;* orcid.org/0000-0001-9097-0630

Fernando A. Soto − *Penn State Greater Allegheny, McKeesport, Pennsylvania 15132, United States*

Janika Wagner − *Institute for Applied Materials − Electrochemical Technologies, Karlsruhe Institute of Technology, Karlsruhe 76131, Germany*

Florian Baakes − *Institute for Applied Materials − Electrochemical Technologies, Karlsruhe Institute of Technology, Karlsruhe 76131, Germany*

Ningxuan Guo − *McCloskey Laboratory, University of California, Berkeley, California 94720, United States*

Francisco Ospina-Acevedo − *Department of Chemical Engineering, Texas A&M University, College Station, Texas 77843, United States*

Fridolin Röder − *Bavarian Center for Battery Technology (BayBatt), University of Bayreuth, 95448 Bayreuth, Germany;* orcid.org/0000-0002-1547-3885

Complete contact information is available at: https://pubs.acs.org/10.1021/acs.jpcc.2c05898

Author Contributions

The manuscript was written through contributions of all authors. All authors have given approval to the final version of the manuscript.

Funding

The authors acknowledge the financial support by the German Federal Ministry of Education and Research through funding the project "Lillint − Thermodynamic and kinetic stability of the Lithium-Liquid Electrolyte Interface" (03XP0225F), the German Research Foundation (DFG) via "SiMET − Simulation of Mechano-Electro-Thermal Processes" (281041241), and the German Academic Exchange Service (DAAD).

Notes

The authors declare no competing financial interest.

ACKNOWLEDGMENTS

Supercomputer resources from the Texas A&M University High Performance Computer Center and Texas Advanced Computing Center (TACC) are gratefully acknowledged.

ABBREVIATIONS

AIMD: Ab Initio Molecular Dynamics; DFT: Density Functional Theory; DMC: Dimethyl Carbonate; EC: Ethylene Carbonate; EIS: Electrochemical Impedance Spectroscopy; KMC: Kinetic Monte Carlo; MD: Molecular Dynamics; SEI: Solid Electrolyte Interface

SYMBOLS

Symbol	unit, definition
C_A	$Ah·m^{-2}$, area specific capacity
C_m	$Ah·g^{-1}$, mass specific capacity
c	$mol·L^{-1}$, concentration
d	m, diameter
E_a	J/mol, activation energy
G	J/mol, free energy
h	layer number (height in z-direction)
k	s^{-1}, reaction constant
k_0	s^{-1}, frequency factor
k_b	$J·K^{-1}$, Boltzmann constant
l	m, box length
Δl	m, distance between two lateral sites
N	number of particles
N_a	Avogadro's number
$\mathcal{P}$	probability
p_h	fraction of a compound in the SEI at a layer height h
p_{ll}	probability of an electron tunnelling at the layer h_{ll}
R	$J·mol^{-1}·K^{-1}$, gas constant
T	°C, temperature
W	s^{-1}, transition rate
x	m, x coordinate
y	m, y coordinate
z	m, z coordinate

GREEK SYMBOLS

Symbol	unit, definition
η	$kg·m^{-1}·s^{-1}$, dynamic viscosity
λ	distance variable
ξ	random number
ϱ	$g·cm^{-3}$, density
σ	electron factor

SUPERSCRIPTS AND SUBSCRIPTS

Symbol	definition
b	backward
cl	clustering
d	diffusion
f	forward
ll	last lithium layer
r	reaction
x	x-coordinate
y	y-coordinate
z	z-coordinate

REFERENCES

(1) Cheng, X. B.; Zhang, Q. Dendrite-Free Lithium Metal Anodes: Stable Solid Electrolyte Interphases for High-Efficiency Batteries. *J. Mater. Chem. A Mater.* **2015**, *3* (14), 7207−7209.

(2) Cheng, X. B.; Zhang, R.; Zhao, C. Z.; Zhang, Q. Toward Safe Lithium Metal Anode in Rechargeable Batteries: A Review. *Chem. Rev.* **2017**, *117* (15), 10403−10473.

(3) Selis, L. A.; Seminario, J. M. Dendrite Formation in Li-Metal Anodes: An Atomistic Molecular Dynamics Study. *RSC Adv.* **2019**, *9* (48), 27835−27848.

(4) Tikekar, M. D.; Choudhury, S.; Tu, Z.; Archer, L. A. Design Principles for Electrolytes and Interfaces for Stable Lithium-Metal Batteries. *Nat. Energy* **2016**, *1* (9), 16114.
(5) Liu, B.; Zhang, J. G.; Xu, W. Advancing Lithium Metal Batteries. *Joule* **2018**, *2* (5), 833−845.
(6) Lin, D.; Liu, Y.; Pei, A.; Cui, Y. Nanoscale Perspective: Materials Designs and Understandings in Lithium Metal Anodes. *Nano Res.* **2017**, *10* (12), 4003−4026.
(7) Peled, E. Film Forming Reaction at the Lithium/Electrolyte Interface. *J. Power Sources* **1983**, *9* (3), 253−266.
(8) Horstmann, B.; Shi, J.; Amine, R.; Werres, M.; He, X.; Jia, H.; Hausen, F.; Cekic-Laskovic, I.; Wiemers-Meyer, S.; Lopez, J.; Galvez-Aranda.; et al. Strategies towards Enabling Lithium Metal in Batteries: Interphases and Electrodes. *Energy Environ. Sci.* **2021**, *14* (10), 5289−5314.
(9) Fang, C.; Wang, X.; Meng, Y. S. Key Issues Hindering a Practical Lithium-Metal Anode. *Trends Chem.* **2019**, *1* (2), 152−158.
(10) An, S. J.; Li, J.; Daniel, C.; Mohanty, D.; Nagpure, S.; Wood, D. L. The State of Understanding of the Lithium-Ion-Battery Graphite Solid Electrolyte Interphase (SEI) and Its Relationship to Formation Cycling. *Carbon N Y* **2016**, *105*, 52−76.
(11) Xu, R.; Zhang, X. Q.; Cheng, X. B.; Peng, H. J.; Zhao, C. Z.; Yan, C.; Huang, J. Q. Artificial Soft−Rigid Protective Layer for Dendrite-Free Lithium Metal Anode. *Adv. Funct Mater.* **2018**, *28* (8), 1705838.
(12) Zhuang, G. v.; Ross, P. N. Analysis of the Chemical Composition of the Passive Film on Li-Ion Battery Anodes Using Attentuated Total Reflection Infrared Spectroscopy. *Electrochem. Solid-State Lett.* **2003**, *6* (7), A136−A139.
(13) Verma, P.; Maire, P.; Novák, P. A Review of the Features and Analyses of the Solid Electrolyte Interphase in Li-Ion Batteries. *Electrochim. Acta* **2010**, *55* (22), 6332−6341.
(14) He, X.; Bresser, D.; Passerini, S.; Baakes, F.; Krewer, U.; Lopez, J.; Mallia, C. T.; Shao-Horn, Y.; Cekic-Laskovic, I.; Wiemers-Meyer, S.; Soto, F. A.; et al. The Passivity of Lithium Electrodes in Liquid Electrolytes for Secondary Batteries. *Nat. Rev. Mater.* **2021**, *6* (11), 1036−1052.
(15) Baakes, F.; Lüthe, M.; Gerasimov, M.; Laue, V.; Röder, F.; Balbuena, P. B.; Krewer, U. Unveiling the Interaction of Reactions and Phase Transition during Thermal Abuse of Li-Ion Batteries. *J. Power Sources* **2022**, *522*, 230881.
(16) Zhang, S. S. A Review on Electrolyte Additives for Lithium-Ion Batteries. *J. Power Sources* **2006**, *162*, 1379−1394.
(17) Lim, K.; Fenk, B.; Popovic, J.; Maier, J. Porosity of Solid Electrolyte Interphases on Alkali Metal Electrodes with Liquid Electrolytes. *ACS Appl. Mater. Interfaces* **2021**, *13* (43), 51767−51774.
(18) Witt, D.; Röder, F.; Krewer, U. Analysis of Lithium-Ion Battery State and Degradation via Physicochemical Cell and SEI Modeling. *Batter Supercaps* **2022**, *5* (7), e20220006.
(19) Hao, F.; Verma, A.; Mukherjee, P. P. Mechanistic Insight into Dendrite-SEI Interactions for Lithium Metal Electrodes. *J. Mater. Chem. A Mater.* **2018**, *6* (40), 19664−19671.
(20) Li, Q.; Pan, H.; Li, W.; Wang, Y.; Wang, J.; Zheng, J.; Yu, X.; Li, H.; Chen, L. Homogeneous Interface Conductivity for Lithium Dendrite-Free Anode. *ACS Energy Lett.* **2018**, *3* (9), 2259−2266.
(21) Harting, N.; Wolff, N.; Röder, F.; Krewer, U. Nonlinear Frequency Response Analysis (NFRA) of Lithium-Ion Batteries. *Electrochim. Acta* **2017**, *248*, 133−139.
(22) Harting, N.; Schenkendorf, R.; Wolff, N.; Krewer, U. State-of-Health Identification of Lithium-Ion Batteries Based on Nonlinear Frequency Response Analysis: First Steps with Machine Learning. *Applied Sciences* **2018**, *8*, 821.
(23) Cheng, X. B.; Zhang, R.; Zhao, C. Z.; Wei, F.; Zhang, J. G.; Zhang, Q. A Review of Solid Electrolyte Interphases on Lithium Metal Anode. *Advanced Science* **2016**, *3*, 1500213.
(24) Ospina-Acevedo, F.; Guo, N.; Balbuena, P. B. Lithium Oxidation and Electrolyte Decomposition at Li-Metal/Liquid Electrolyte Interfaces. *J. Mater. Chem. A Mater.* **2020**, *8* (33), 17036−17055.
(25) Aurbach, D. Review of Selected Electrode-Solution Interactions Which Determine the Performance of Li and Li Ion Batteries. *J. Power Sources* **2000**, *89* (2), 206−218.
(26) Edström, K.; Herstedt, M.; Abraham, D. P. A New Look at the Solid Electrolyte Interphase on Graphite Anodes in Li-Ion Batteries. *J. Power Sources* **2006**, *153* (2), 380−384.
(27) Shiraishi, S.; Kanamura, K.; Takehara, Z. I. Influence of Initial Surface Condition of Lithium Metal Anodes on Surface Modification with HF. *J. Appl. Electrochem.* **1999**, *29* (7), 867−881.
(28) Peled, E. The Electrochemical Behavior of Alkali and Alkaline Earth Metals in Nonaqueous Battery Systems—The Solid Electrolyte Interphase Model. *J. Electrochem. Soc.* **1979**, *126* (12), 2047.
(29) Owejan, J. E.; Owejan, J. P.; Decaluwe, S. C.; Dura, J. A. Solid Electrolyte Interphase in Li-Ion Batteries: Evolving Structures Measured in Situ by Neutron Reflectometry. *Chem. Mater.* **2012**, *24* (11), 2133−2140.
(30) Ramos-Sanchez, G.; Soto, F. A.; Martinez De La Hoz, J. M.; Liu, Z.; Mukherjee, P. P.; El-Mellouhi, F.; Seminario, J. M.; Balbuena, P. B. Computational Studies of Interfacial Reactions at Anode Materials: Initial Stages of the Solid-Electrolyte-Interphase Layer Formation. *Journal of Electrochemical Energy Conversion and Storage* **2016**, *13* (3), 1−10.
(31) Soto, F. A.; Martinez de la Hoz, J. M.; Seminario, J. M.; Balbuena, P. B. Modeling Solid-Electrolyte Interfacial Phenomena in Silicon Anodes. *Curr. Opin Chem. Eng.* **2016**, *13*, 179−185.
(32) Camacho-Forero, L. E.; Smith, T. W.; Balbuena, P. B. Effects of High and Low Salt Concentration in Electrolytes at Lithium-Metal Anode Surfaces. *J. Phys. Chem. C* **2017**, *121* (1), 182−194.
(33) Martinez De La Hoz, J. M.; Soto, F. A.; Balbuena, P. B. Effect of the Electrolyte Composition on SEI Reactions at Si Anodes of Li Ion Batteries. *J. Phys. Chem. C* **2015**, *119* (13), 7060−7068.
(34) Bertolini, S.; Balbuena, P. B. Buildup of the Solid Electrolyte Interphase on Lithium-Metal Anodes: Reactive Molecular Dynamics Study. *J. Phys. Chem. C* **2018**, *122* (20), 10783−10791.
(35) von Kolzenberg, L.; Latz, A.; Horstmann, B. Chemo-Mechanical Model of SEI Growth on Silicon Electrode Particles. *Batter Supercaps* **2022**, *5* (2), 1−11.
(36) Röder, F.; Braatz, R. D.; Krewer, U. Multi-Scale Simulation of Heterogeneous Surface Film Growth Mechanisms in Lithium-Ion Batteries. *J. Electrochem. Soc.* **2017**, *164* (11), E3335−E3344.
(37) Methekar, R. N.; Northrop, P. W. C.; Chen, K.; Braatz, R. D.; Subramanian, V. R. Kinetic Monte Carlo Simulation of Surface Heterogeneity in Graphite Anodes for Lithium-Ion Batteries: Passive Layer Formation. *Proceedings of the American Control Conference* **2011**, *158* (4), A363−A370.
(38) Abbott, J. W.; Hanke, F. Kinetically Corrected Monte Carlo-Molecular Dynamics Simulations of Solid Electrolyte Interphase Growth. *J. Chem. Theory Comput* **2022**, *18* (2), 925−934.
(39) Sitapure, N.; Lee, H.; Ospina-Acevedo, F.; Balbuena, P. B.; Hwang, S.; Kwon, J. S. I. A Computational Approach to Characterize Formation of a Passivation Layer in Lithium Metal Anodes. *AIChE J.* **2021**, *67*, e17073.
(40) Röder, F.; Braatz, R. D.; Krewer, U. Multi-Scale Modeling of Solid Electrolyte Interface Formation in Lithium-Ion Batteries. *Comput.-Aided Chem. Eng.* **2016**, *38*, 157−162.
(41) Röder, F.; Laue, V.; Krewer, U. Model Based Multiscale Analysis of Film Formation in Lithium-Ion Batteries. *Batter Supercaps* **2019**, *2* (3), 248−265.
(42) Nagaoka, M.; Suzuki, Y.; Okamoto, T.; Takenaka, N. A Hybrid MC/MD Reaction Method with Rare Event-Driving Mechanism: Atomistic Realization of 2-Chlorobutane Racemization Process in DMF Solution. *Chem. Phys. Lett.* **2013**, *583*, 80−86.
(43) Takenaka, N.; Bouibes, A.; Yamada, Y.; Nagaoka, M.; Yamada, A. Frontiers in Theoretical Analysis of Solid Electrolyte Interphase Formation Mechanism. *Adv. Mater.* **2021**, *33* (37), 2100574.
(44) Xu, K. Electrolytes and Interphases in Li-Ion Batteries and Beyond. *Chem. Rev.* **2014**, *114* (23), 11503−11618.
(45) Wang, Y.; Nakamura, S.; Ue, M.; Balbuena, P. B. Theoretical Studies to Understand Surface Chemistry on Carbon Anodes for

https://doi.org/10.1021/acs.jpcc.2c05898
J. Phys. Chem. C 2023, 127, 4872−4886

Lithium-Ion Batteries: Reduction Mechanisms of Ethylene Carbonate. *J. Am. Chem. Soc.* **2001**, *123* (47), 11708−11718.
(46) Soto, F. A.; Ma, Y.; Martinez De La Hoz, J. M.; Seminario, J. M.; Balbuena, P. B. Formation and Growth Mechanisms of Solid-Electrolyte Interphase Layers in Rechargeable Batteries. *Chem. Mater.* **2015**, *27* (23), 7990−8000.
(47) Tasaki, K.; Goldberg, A.; Lian, J.-J.; Walker, M.; Timmons, A.; Harris, S. J. Solubility of Lithium Salts Formed on the Lithium-Ion Battery Negative Electrode Surface in Organic Solvents. *J. Electrochem. Soc.* **2009**, *156* (12), A1019.
(48) Stich, M.; Göttlinger, M.; Kurniawan, M.; Schmidt, U.; Bund, A. Hydrolysis of LiPF6 in Carbonate-Based Electrolytes for Lithium-Ion Batteries and in Aqueous Media. *J. Phys. Chem. C* **2018**, *122* (16), 8836−8842.
(49) Tornheim, A.; Sahore, R.; He, M.; Croy, J. R.; Zhang, Z. Preformed Anodes for High-Voltage Lithium-Ion Battery Performance: Fluorinated Electrolytes, Crosstalk, and the Origins of Impedance Rise. *J. Electrochem. Soc.* **2018**, *165* (14), A3360−A3368.
(50) Perez Beltran, S.; Balbuena, P. B. SEI Formation Mechanisms and Li+ Dissolution in Lithium Metal Anodes: Impact of the Electrolyte Composition and the Electrolyte-to-Anode Ratio. *J. Power Sources* **2022**, *551*, 232203.
(51) Hamann, C. H.; Vielstich, W. *Elektrochemie*, 4. Auflage.; Wiley-VCH Verlag GmbH & Co KgaA: Weinheim, 2005.
(52) Voter, A. F. *Introduction To the Kinetic Monte Carlo Method*; Los Alamos, 2007. DOI: 10.1007/978-1-4020-5295-8_1.
(53) Doll, K.; Harrison, N. M.; Saunders, V. R. A Density Functional Study of Lithium Bulk and Surfaces. *J. Phys.: Condens. Matter* **1999**, *11* (26), 5007−5019.
(54) Mortimer, C. E.; Müller, U. *Chemie*, 11th ed.; Thieme: Stuttgart, New York, 2014.
(55) Kratzer, P. Monte Carlo and Kinetic Monte Carlo Methods. *arXiv:0904.2556 [cond-mat.mtrl-sci]* **2009**, na.
(56) Soto, F. A.; Balbuena, P. B. Elucidating Oligomer-Surface and Oligomer-Oligomer Interactions at a Lithiated Silicon Surface. *Electrochim. Acta* **2016**, *220*, 312−321.
(57) Eyring, H. The Activated Complex in Chemical Reactions. *J. Chem. Phys.* **1935**, *3* (2), 107.
(58) Ibach, H. *Physics of Surfaces and Interfaces*; Springer Berlin: Heidelberg, 2006. DOI: 10.1007/3-540-34710-0.
(59) Neuhaus, J.; Bellaire, D.; Kohns, M.; von Harbou, E.; Hasse, H. Self-Diffusion Coefficients in Solutions of Lithium Bis-(Fluorosulfonyl)Imide with Dimethyl Carbonate and Ethylene Carbonate. *Chem. Ing. Tech.* **2019**, *91* (11), 1633−1639.
(60) Schwoebel, R. L.; Shipsey, E. J. Step Motion on Crystal Surfaces. *J. Appl. Phys.* **1966**, *37* (10), 3682−3686.
(61) Jansen, A. P. J. *An Introduction To Monte Carlo Simulations Of Surface Reactions*; Springer: New York, 2003.
(62) Andersson, A. M.; Henningson, A.; Siegbahn, H.; Jansson, U.; Edström, K. Electrochemically Lithiated Graphite Characterised by Photoelectron Spectroscopy. *J. Power Sources* **2003**, *119*−*121*, 522−527.
(63) Westley, F.; United States National Bureau of Standards; National Measurement Laboratory (U.S.). *Table of Recommended Rate Constants for Chemical Reactions Occurring in Combustion*; United States Government Printing Office: Washington D.C., 1980.
(64) MathWorks. *MATLAB* (Version R2020b, Update 2); Natick, MA, 2020.
(65) Reniers, J. M.; Mulder, G.; Howey, D. A. Review and Performance Comparison of Mechanical-Chemical Degradation Models for Lithium-Ion Batteries. *J. Electrochem. Soc.* **2019**, *166* (14), A3189−A3200.
(66) von Kolzenberg, L.; Latz, A.; Horstmann, B. Solid−Electrolyte Interphase During Battery Cycling: Theory of Growth Regimes. *ChemSusChem* **2020**, *13* (15), 3901−3910.
(67) Liu, Z.; Lu, P.; Zhang, Q.; Xiao, X.; Qi, Y.; Chen, L. Q. A Bottom-Up Formation Mechanism of Solid Electrolyte Interphase Revealed by Isotope-Assisted Time-of-Flight Secondary Ion Mass Spectrometry. *J. Phys. Chem. Lett.* **2018**, *9* (18), 5508−5514.
(68) Lin, Y. X.; Liu, Z.; Leung, K.; Chen, L. Q.; Lu, P.; Qi, Y. Connecting the Irreversible Capacity Loss in Li-Ion Batteries with the Electronic Insulating Properties of Solid Electrolyte Interphase (SEI) Components. *J. Power Sources* **2016**, *309*, 221−230.
(69) Wang, A.; Kadam, S.; Li, H.; Shi, S.; Qi, Y. Review on Modeling of the Anode Solid Electrolyte Interphase (SEI) for Lithium-Ion Batteries. *NPJ. Comput. Mater.* **2018**, *4*, 15.
(70) Albertus, P.; Babinec, S.; Litzelman, S.; Newman, A. Status and Challenges in Enabling the Lithium Metal Electrode for High-Energy and Low-Cost Rechargeable Batteries. *Nat. Energy* **2018**, *3* (1), 16−21.

https://doi.org/10.1021/acs.jpcc.2c05898
J. Phys. Chem. C 2023, 127, 4872−4886